Ultrasonically Recovered Performance of γ-Irradiated Metal-Silicon Structures

Alla M. Gorb, Oleg A. Korotchenkov, Oleg Ya. Olikh, and Artem O. Podolian

***Abstract*—The MHz-frequency ultrasound treatment is shown to offer a recovery tool in the current-voltage ($I-V$) characteristics of the γ-irradiated metal-silicon structures. Experimental observations of the ultrasound treatment effect on the carrier transport and photocurrent transient parameters are highlighted. It is shown that up to 30% of the Schottky diode currents and free carrier lifetimes worsen by the irradiation could be recovered in the stress field of ultrasound. The likely scenario behind the treatment effect is outlined, implying the involvement of the vacancies released from the E-centers and subsequently trapped at the Si-SiO_2 interface. It is shown that the technique enables near-room temperature modification of electronic properties of metal-semiconductor Schottky diodes and metal-oxide-semiconductor devices. The density of the electrically active bulk and interface traps can be controllably tuned using this technique. Potential relevance of the processing approach in the context of applications in electronics and detector technologies is pointed out.**

***Index Terms*—Defects, lifetime, radiation, silicon, ultrasound.**

I. Introduction

SILICON is widely used in radiation detectors and electronic devices, and numerous fields of application imply adverse radiation environments that may affect the operation of the devices [1]. Metal-semiconductor Schottky diodes and metal-oxide-semiconductor (MOS) diodes are particularly sensitive to high-level radiations, e.g., to ^{60}Co γ-rays [2], [3]. The formation of lattice defects in the form of vacancies, defect clusters and dislocation loops near the metal-semiconductor interface caused by the irradiation is very harmful for device performance since these defects can act as recombination and trapping centers for charge carriers. Therefore, it is of special interest to develop reliable techniques capable of reducing the number of the electrically active damage defect centers introduced by irradiation. Elevated temperatures are commonly employed in the defect annealing techniques, which inherently pose serious problems of generating thermal donor centers (see [4] and references therein), contaminating a semiconductor in the metal-semiconductor structure due to diffusion of the metal contact material, etc.

Numerous defects located in the bulk and at the Si-SiO_2 interface most relevant for device reliability are the ones which are electrically active, capable of trapping or exchanging charges. Thus, neutral defects are hazardous as they can trap charge during the device working cycle, leading to an accelerating aging. On the other hand, charged defects in the oxide bulk or at the Si-SiO_2 interface influence metal-oxide-semiconductor field-effect transistor (MOSFET) device performance such as threshold voltage of the drain current in the ohmic regime [5], [6]. It is well known that the oxide traps (N_{ot}) and Si-SiO_2 interface traps (N_{it}) are dominant for the degradation of the current-voltage ($I-V$) characteristics in irradiated MOSFETs. Exposure of MOS capacitors to ionizing radiation generates positive charge in the oxide layer and E$'$ centers, resulting from an oxygen vacancy in SiO_2 [7]–[9]. The positive charge can be removed by low-temperature (< 400°C) thermal annealing. It is well known, that nuclear radiation also produces neutral electron traps [10], which cannot be removed by the same annealing. Controlling N_{it} provides a useful way to reduce the harmful effects of lifetime and quantum efficiency degradation in silicon photodiodes [11].

Interface-trap generation is also an important reliability concern in MOSFETs subjected to a negative bias temperature instability, Fowler-Nordheim, and hot-carrier injection stress [12]–[14]. It was reported that the mechanism of N_{it} generation during stress and any recovery of N_{it} after stress must be properly understood for accurate prediction of device lifetime under actual operating conditions.

The treatment of Si with ultrasound (ultrasound treatment, UST) was shown to offer a nearly room-temperature annealing of radiation defects [15]–[18] paving an alternative way to improve the performance of silicon-based devices for particle physics experiments, nuclear medicine and space. A lot of effort has been put into the exploitation of the UST technique in order to engineer and to recover defect-related electronic parameters of silicon [19], [20].

The ultrasound treatment utilized in this work was purpose-built to facilitate the UST concept as a recovery tool in the current-voltage characteristics of the γ-irradiated metal-silicon structures. The next purpose of this work was to introduce the relevant mechanism driving the observed evolution of the $I-V$ characteristics. Understanding of UST effects on irradiated metal-silicon structures would have an impact on the design of the diode devices allowing the development of a specific method for an enhanced radiation stability of these types of semiconductor devices.

II. Experimental

EXPERIMENTS were performed on n-type (111)-oriented crystalline float-zone Si with residual boron (B) impurity concentration of about 10^{12} cm^{-3} and doping phosphorus (P) impurity concentration of 2×10^{12} cm^{-3}. The corresponding

Manuscript received September 07, 2009; revised February 12, 2010; accepted March 05, 2010. Date of current version June 16, 2010. This work was supported in part by the Ministry of Education and Science of Ukraine.

The authors are with the Department of Physics, Taras Shevchenko Kyiv National University, Kyiv 01601, Ukraine (e-mail: g_alla@ukr.net).

Color versions of one or more of the figures in this paper are available online at http://ieeexplore.ieee.org.

Digital Object Identifier 10.1109/TNS.2010.2047655

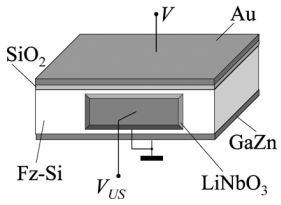

Fig. 1. Schematics of the investigated structure.

resistivity is 4 $\mathrm{k\Omega \cdot cm}$. A bulk silicon material was divided into several rectangular-shaped samples of approximately $1 \times 5 \times 10\ \mathrm{mm^3}$. One of the samples was used as the reference materials, the other ones were γ-irradiated ($^{60}\mathrm{Co}$ source) at nominal room temperature to the dose ranged from 5×10^6 to 5×10^7 rad. The resulting conductivity of the samples was reduced to about 0.5 of the initial value. They were found to remain n-type at all irradiation doses used.

The sample geometry is sketched Fig. 1. The Schottky barrier structures, used in the current-voltage measurements, were prepared by chemical etching of the upper Si surfaces using HF-$\mathrm{HNO_3}$-$\mathrm{CH_3COOH}$ solutions (HF: $\mathrm{HNO_3}$: $\mathrm{CH_3COOH} = 3:5:3$), followed by the surface oxidation due to the exposure to ambient air for 24 hours and the Au vacuum evaporation. GaZn-eutectic Ohmic contacts were rubbed on the bottom surfaces of the samples. A metal-oxide-semiconductor (MOS) device was consequently formed. For the photocurrent (PC) decay measurements, GaZn Ohmic contacts were rubbed on the top and bottom contact layers. The area of the upper contact was $\mathrm{A} \approx 50\ \mathrm{mm^2}$ in all cases.

In this work, ultrasound treatment techniques were used to recover defect-related electronic parameters of the irradiated samples. This was done by attaching the $\mathrm{LiNbO_3}$ piezoelectric transducer to one side of the sample, as shown in Fig. 1. An epoxy glue was used as the bonding medium, providing the rigid coupling of the transducer to the sample. The thickness resonant frequency (f) of the transducers was 4 MHz. A radio-frequency (rf) voltage supplied from a generator drives the transducer, resulting in vibrations of the coupled transducer-sample system. The rf strain is then produced in the semiconductor allowing to mechanically modify the electronic properties of the material.

The density of acoustic energy flux (W_{US}) in Si was estimated by neglecting the mechanical loses in the transducers, $W_{US} = V_{US}^2/R_a$, with V_{US} the rf voltage amplitude applied to the transducer and R_a the resistance of an acoustic irradiation. The value of R_a can be expressed as

$$R_a = \frac{1}{8fK^2C_t} \cdot \frac{Z_s}{Z_t}, \tag{1}$$

where K is the coefficient of electro-mechanical coupling of the transducer, C_t is its capacitance, Z_s and Z_t are the impedance of the sample and the transducer, respectively. Data are given below for $W_{US} \approx 2\ \mathrm{W/cm^2}$, yielding the strain amplitude inside the sample of about 10^{-5}.

The sample temperature was measured with a copper-constantan thermocouple directly attached to the sample surface. Ultrasonic treatment was carried out by a series of consecutive loading-unloading cycles, 30 min each. The sample surface temperature raise did not exceed 350 K at the greatest W_{US} used over the course of the loading cycle.

The characteristics of the Au/Si Schottky barrier diode, after γ-irradiation and after UST, were investigated using an $I-V$ measurement technique. For this purpose, computer-driven system based on the analog-to-digital converter ADA-1282 was used. This setup allows to measure forward and reverse bias $I-V$ characteristics for the current varied in the range from $3 \cdot 10^{-10}$ to 10^{-3} A with a voltage step of 0.01 V.

In order to relate the observed $I-V$ changes to defect annealing processes, the photocurrent transient decays were additionally studied before and after ultrasonic treatments. These were taken using a pump pulse generated by a 1.06-μm light-emitting diode (LED) with a half-width of 50 nm. The LED beam that excites the sample was expanded to achieve nominally uniform illumination on the sample surface. The LED was controlled by the external bias in the form of square-function pulse. Light pulse lengths of 100 μs were used, with rise and fall times of ≈ 1.2 μs. The LED pulse sequence had a period of about 50 ms, which was substantially greater than the PC decay time. The background noise level was obtained by averaging the decay signal in the relaxed transient range. The light pulse intensity was controlled so that the low-level injection conditions were satisfied (the injected carrier concentration was 1% of its steady value). Decay transients were stored in the computer memory using an analog-to-digital converter with a resolution of 2 μs. RC time constants were observed to be less than 100 ns, which was much smaller than the time scales of interest.

The transient PC is due to mobile excess electrons and holes, generated by the light-induced band-to-band transitions. If the decay behavior of electrons and holes is identical, the excess densities of electrons and holes are equal at every instant. This condition is usually satisfied in the low-level carrier injection range, when the charge carrier transport is controlled by the minority carriers. For a uniform distribution of excess carriers the transient photoconductivity $\Delta\sigma(t) = \Delta n(t)(\mu_n + \mu_p)e$, where $\Delta n(t)$ is the excess density of minority carriers, μ_n and μ_p are the mobility of electrons and holes, respectively, and e is the electron charge. A relaxation (decay) time $\tau(t)$ for the excess minority carrier density can be defined as

$$\frac{1}{\tau(t)} = -\frac{1}{\triangle n(t)} \frac{\partial \triangle n(t)}{\partial t}, \tag{2}$$

which is also the decay time of the photoconductivity.

The heat treatments were carried out by isochronal anneals at temperatures ranging between 350 and 530 K in a quartz-tube furnace under ambient conditions.

III. Results and Discussion

A. A Brief Introduction to Carrier Transport Mechanisms

Due to the presence of surface or interface states in the band gap of a semiconductor, the Fermi level at the surface (or interface) may have a different position with respect to the band edges than in the bulk. At thermal equilibrium, the Fermi level is

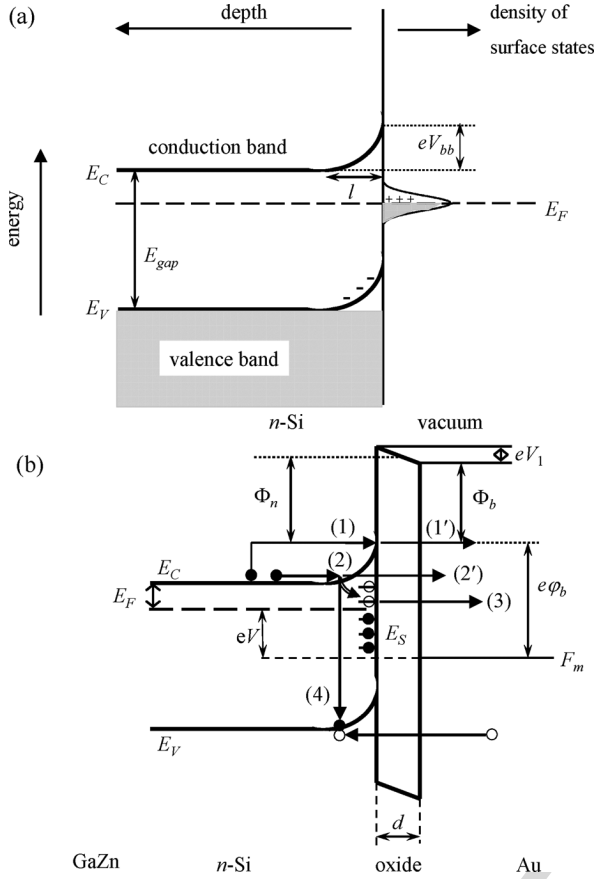

Fig. 2. Band diagrams of MOS devices: (a) in equilibrium, in the absence of the insulating layer, (b) at externally applied voltage V, with the oxide layer of the thickness of d. The diagrams illustrate the band bending V_{bb} in the subsurface region of an n-doped semiconductor which have surface states within the band gap. Φ_b is the Schottky barrier height, Φ_n is the mean barrier height, E_F and F_m are the Fermi levels in Si and Au, respectively, $\Phi_n = \Phi_b + eV_1/2$. Each of the horizontal lines E_S in (b) represents an interface trap. It is either occupied by an electron (solid circle) or occupied by a hole (open circle). Arrows (1)-(4) represent the main carrier transport mechanisms discussed in the text.

constant throughout the crystal, thus yielding a charge transfer between surface and bulk. Consequently, the surface is charged with the charge value which is balanced by an opposite space charge in a layer underneath the surface. Assume that the energetic position and occupancy of the surface states within the band gap is such that the charge transfer depletes the subsurface layer of majority carriers. Then the charge distribution produces an electric field within the space charge region and a corresponding band bending, which can be obtained from Poisson's equation and is shown in Fig. 2. The thickness l of the depletion layer is

$$l = \sqrt{\frac{2\varepsilon\varepsilon_0 V_{bb}}{eN_D}}, \tag{3}$$

where V_{bb} is the magnitude of the band bending, N_D is the bulk dopant concentration, ε is the dielectric constant and ε_0 is the dielectric constant of free space.

The density of a dark current I, flowing between metal and semiconductor, in the n-type semiconductor-based MOS device under a forward bias is as follows [21]

$$I = CP_t(e^{eV_2/nkT} - 1), \tag{4}$$

where V_2 is the voltage drop across the space-charge (depletion) region of the semiconductor, n is the ideality factor, k is the Boltzman constant, T is the temperature, P_t is the carrier transfer probability through the insulating layer, and C is a coefficient.

Furthermore, in the more general case, the current is limited by the series resistance, which is due to the contact resistance between the metal and the semiconductor, the resistance of the thin insulating layer, the resistance of the semiconductor or the resistance of the connecting wires. Since, in high-resistivity Si, the resistance of the semiconductor R_S cannot be neglected, the bias voltage applied to the top metal electrode (cf. Fig. 1) V is

$$V = V_1 + V_2 + IR_S, \tag{5}$$

where V_1 is the voltage drop across the insulating oxide layer, IR_S is the voltage drop across the quasi-neutral region of the semiconductor of width l in Fig. 2(a).

In case of the quantum mechanical tunneling through the insulating layer [processes (1') and (3) in Fig. 2(b)] the probability P_t is

$$P_t = e^{-t\sqrt{\Phi_n}d}, \tag{6}$$

where t is the tunneling constant which is $t = \sqrt{2m^*\hbar}$, m^* is the effective electron mass in SiO_2 ($\sim 0.5\ m_0$), m_0 is the free electron mass, and $\hbar$ is the Planck constant. Overcoming the Schottky barrier by process (1) in Fig. 2(b) can be described in the thermionic emission model, and the coefficient C is given by

$$C = C_{(1)} = A^*T^2e^{-e\varphi_b/kT}, \tag{7}$$

where φ_b is the Schottky barrier height in the semiconductor for the MOS region and A^* is the modified Richardson constant. Then the total current transmitted through the processes (1) and (1') is

$$I_{(1)} = A^*T^2e^{-e\varphi_b/kT}e^{-t\sqrt{\Phi_n}d}(e^{eV_2/nkT} - 1). \tag{8}$$

The ideality factor $n = 1$ if the recombination-generation current developed due to band-to-band recombination/generation [process (4) in Fig. 2(b)] is unimportant, and $1 < n < 2$ otherwise.

Since the doping concentration in our samples is low ($\approx 10^{12}\ \mathrm{cm}^{-3}$), the width of the depleted region l, obtained from (1), is large enough, of about 20 μm. Then there is hardly the Schottky barrier and the insulating layer to tunnel through, and the migration pathway sketched by process (2) in Fig. 2(b)

is likely to be avoided by the carrier in favor of an easier route (1)-(1'). The experimentally observed current may therefore be dominated by process (1)-(1') and the $I_{(2)}$ component can be neglected.

If pathway (1)-(1') in Fig. 2(b) is the dominant process, the mean barrier height Φ_n at the silicon-oxide interface can be calculated from the slope of the semilogarithmic $I-d$ plot. If $V_1 \ll V_2$, the logarithmic plot of $I/[1-\exp(-eV/nkT)]$ against V is linear. In this case, $A^*T^2 \cdot e^{-e\varphi_b/kT}$ can be obtained from the I-axis intercept at zero V, and from this the barrier height φ_b can be derived.

The effect of tunnelling through the interface states E_S [process (3) in Fig. 2(b)] can be achieved by introducing the density D_S of the interface states, which are evenly distributed in the energy range ΔE_S, the capture cross-section σ_{St} of the interface states for tunnelling, and the occupational probability f_S of the interface states. In this process, the electrons, captured at the interface states [curved arrow in Fig. 2(b)], tunnel from these states to vacant states in the metal (Au). A backward tunnelling of electrons from the metal to the interface states should also be taken into account. Then the current is [22]

$$I_{(3)} = eD_S F_S \sigma_{St} \upsilon_m g(E_S) \Delta E_S \cdot e^{-t\sqrt{\Phi_S}d} \times (1 - e^{-eV_1/kt}), \tag{9}$$

where υ_m is the thermal velocity of electrons in the metal, $g(E_S)$ is the density of states in the metal at the energy of E_S, and Φ_S is the barrier height for electrons captured at the interface states.

Obviously, in the general case, the current through the MOS device is equal to the algebraic sum of $I_{(1)}$, $I_{(2)}$ and the current $I_{(3)}$ due to tunnelling via the interface states. This, of course, complicates the analysis of the measured $I-V$ curves.

B. Change in the Carrier Transport and Photocurrent Transient Parameters of Irradiated MOS Structures

Fig. 3 shows the semilogarithmic plots of the forward- and reverse-bias $I-V$ characteristics of one of the MOS structures, taken before and after γ-irradiation (solid and open circles, respectively). It is seen that the plot taken before γ-irradiation consists of a good linear range with a well-defined intermediate-bias region followed by the current saturation. In contrast, the intermediate-bias region with different slopes is achieved in the irradiated sample at much lower voltages, thus making a linear range less pronounced and decreasing substantially the value of the saturation current.

These experimental results can be interpreted in the light of the above models. The forward $I-V$ curves shown in Fig. 3 can be analyzed using the Schottky barrier thermionic emission model, so that

$$I = I_S(e^{e(V-IR_S)/nkT} - 1), \tag{10}$$

which is derived from (8) under the simplifying assumption that $V_1 \ll V_2$ and introducing the saturation current $I_S = AA^*T^2 e^{-e\varphi_b/kT} e^{-t\sqrt{\Phi_n}d}$.

The results of simulations shown by solid curves in the inset of Fig. 3 reveal a very good correspondence between the

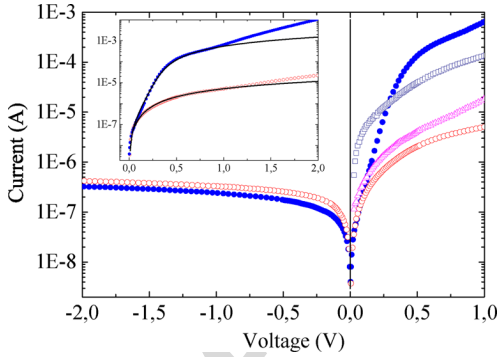

Fig. 3. The reverse and forward $I-V$ curves of the Au-SiO_2-Si Schottky barrier structure taken before (solid circles) and after (open circles) γ-irradiation. $T = 295$ K. Inset enlarges the forward bias region, the solid lines are the fitting curves calculated by using (9) with $I_S = 5 \times 10^{-8}$ A, $R_S = 10^3\ \Omega$ (upper curve) and $1.5 \times 10^5\ \Omega$ (lower curve). Effect of ultrasound treatment is illustrated by triangles (30-min UST) and squares (60-min).

measured and computed $I-V$ characteristics at $V \leq 1$ V, with the discrepancies which arise at greater voltages. Within a schematic picture shown in Fig. 2(b) this result may be interpreted such that two different processes (1) and (1') are present in the electron pathway. Indeed, the current saturation is achieved at the condition when the V-dependent resistance of the depleted region approaches the sum of R_S and the resistance of the oxide layer, which is achieved at about 0.4 V in the pre-irradiated sample. Increasing V imposes decreased band bending and width of the depletion region (eV_{bb} and l in Fig. 2(a), respectively), thus enhancing the electron capture probability at the interface states. Then the current through process (3) in Fig. 2(b) turns out to be favorable, which may lead to increased current above ≈ 1 V observed in the inset of Fig. 3.

Furthermore, as the applied voltage V increases above ≈ 1.6 V, the charge density at the interface becomes so high that it leaks through the oxide by Fowler-Nordheim or direct tunneling mechanism, which can be described by [23]

$$I = A\frac{e^3}{16\pi^2\hbar\Phi_n}\frac{m_0}{m^*}\left(\frac{V}{d}\right)^2 \exp\left(-\frac{4\sqrt{2m^*}}{3e\hbar}\frac{d}{V}\Phi_n^{3/2}\right), \tag{11}$$

where A is the tunneling area. It is observed that the Fowler-Nordheim plot of $\ln(I/V^2)$ *vs* $1/V$ clearly exhibits a linear relationship above ≈ 1.6 V. Therefore, the above discrepancies can also be due to electron tunneling at a large bias, which subsequently increases the measured current.

Since γ-irradiation causes the increase in the sample resistance R_S, the saturation condition, $V_2 \approx V_1 + IR_S$, is achieved at a lower voltage V, applied to the structure. This leads to a decrease in the saturation current in the irradiated sample, as observed both experimentally and theoretically in Fig. 3. However, the increase in the fitting value of R_S for the curves shown in the inset of Fig. 3 is substantially greater than the measured resistivity enhancement (about two times greater) observed after irradiation. More detailed understanding of the structural and compositional complexity of oxide layers grown on the irradiated surface seems to be necessary to reveal in order to account

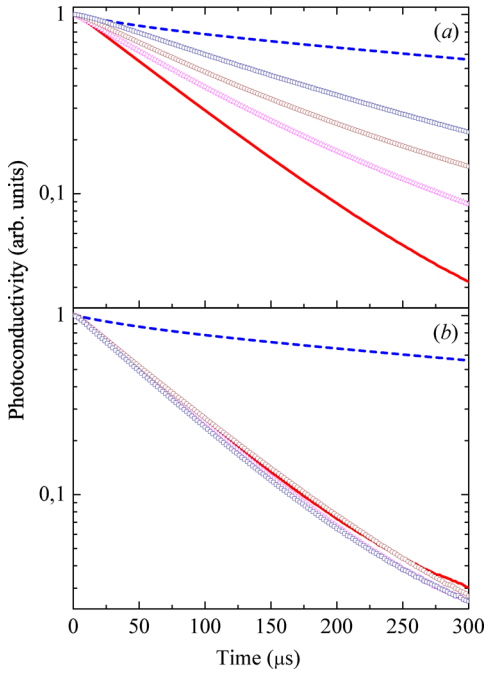

Fig. 4. Photocurrent transient decays taken before (dotted curves) and after (solid curves) γ-irradiation (5×10^6 rad), and after ultrasound *(a)* and thermal *(b)* treatments of the irradiated sample. UST is performed during 60 (triangles), 120 (circles) and 240 (squares) min. Thermal treatment is performed at 360 K during 60 (triangles), 120 (circles) and 240 (squares) min. The surface recombination velocity is kept constant at about $S = 10^3$ cm/s. The carrier lifetime $\tau = 500(1), 77(2), 100(3), 119(4)$ and 177 μs (5).

correctly for an increased resistance of the oxide layer grown on the irradiated surface.

At reverse bias, a square-root dependence $I_R \sim \sqrt{V}$ is observed for V $>$ 1 V, signifying that the generation-recombination process [process (4) in Fig. 2(b)] determines the current mechanism. Indeed, the reverse current is [24]

$$I_R = \frac{eAn_i l}{2\tau}, \tag{12}$$

where n_i is the charge carrier concentration in the intrinsic semiconductor and τ is the free carrier lifetime with respect to recombination and trapping in the depleted region. Since $l \sim \sqrt{V_{bb} + V_2}$, the square-root dependence is expected for the generation-recombination process, which is indeed observed experimentally.

Changes in τ can be obtained from PC decay measurements shown in Fig. 4. The decays are nearly simple exponentials with the measured lifetimes τ, which are effective lifetimes integrating bulk (τ_b) and surface (τ_s) recombination components [25]:

$$\frac{1}{\tau} = \frac{1}{\tau_b} + \frac{1}{\tau_s} = \frac{1}{\tau_b} + \pi^2 D \left(\frac{\xi^2}{l_1^2} + \frac{\eta^2}{l_2^2} + \frac{\zeta^2}{l_3^2} \right), \tag{13}$$

TABLE I
ULTRASOUND MODIFICATION OF THE RECTIFICATION FACTOR OF THE MOS DEVICE TAKEN AT $V = 0.35$ V AND OF THE FREE CARRIER LIFETIME τ OBTAINED FROM THE PHOTOCURRENT DECAY.

Parametr	ST duration (min)		
	0	30	60
k_r	0.3	1.6	85
τ_1/τ_{01}	1	1.2	1.4
τ_2/τ_{02}	1	-	1.3

τ_{01} and τ_1 are the carrier lifetimes in the irradiated and subsequently ultrasound treated structure, respectively, obtained from Eq. (12). τ_2 and τ_{02} are the ones obtained from the photocurrent decays.

where D is the diffusion coefficient of the minority carrier, l_1, l_2 and l_3 are the linear dimensions of the sample, and ξ, η and ζ are determined from the following characteristic equations:

$$cot\left(\frac{\xi\pi}{2}\right) = \frac{\xi\pi D}{Sd_1}, cot\left(\frac{\eta\pi}{2}\right) = \frac{\eta\pi D}{Sd_2}, cot\left(\frac{\zeta\pi}{2}\right) = \frac{\zeta\pi D}{Sd_3} \tag{14}$$

with S the surface recombination velocity. Therefore, if the surface effect is fixed by fixing S the values of τ obtained in Fig. 4 exhibit the bulk lifetimes τ_b.

Irradiation produces a considerable decrease in the carrier lifetime, as evidenced by comparing dotted and solid curves in Fig. 4, which is indicative of enhanced defect concentrations in the structures. The latter is due to the fact that γ-irradiation produces vacancies and self-interstitials, which may combine with impurities to form complexes of defects. These can act as efficient recombination centers yielding the observed shortening of the minority carrier lifetime. The thermal annealing behavior of the lifetime (not shown here) can qualitatively be described as due to at least two types of defects, which anneal by ≈ 150 and 225°C. The former lifetime recovery stage correlates with the E-center (vacancy V trapped at atom P) anneal [26], whereas the latter one would come from the anneal of the divacancy V_2 [27].

Hence there appears to be an interplay between the terms describing the variation of the reverse current in (12). The observed decrease in τ and decrease in the thickness l of the depletion layer with increasing defect concentration in the irradiated structure likely to result in enhanced I_R seen in Fig. 3 (open circles).

C. Ultrasound Treatment Effect on the Carrier Transport and Photocurrent Transient Parameters

The effect of UST on the forward $I - V$ characteristics is shown in Fig. 3 by triangles and squares. The reverse currents are also affected by ultrasound, and the effect on the carrier transport parameters can be explicitly illustrated in terms of the rectification factor k_r of the structure, which is defined as the ratio of the forward and the reverse currents (see Table I).

It turned out that the most essential features of UST are the remarkable increase of the forward currents (triangles and squares in Fig. 3) and of the diode rectification factor (k_r in Table I). The latter is in part due to the increase in τ (data of Table I) and the subsequent decrease in the reverse current, both of which are observed experimentally. The lifetime increase due to UST is exemplified by a slowing down the decay curves shown by triangles, circles and squares in Fig. 4(a). Because the magnitude

of the reverse current is inversely proportional to τ, the current is found to decrease with UST in a way that is prescribed by (12).

Of prime importance is the fact that the sample exposure to thermal treatments at 360 K, which is slightly greater than the highest possible value of the sample temperature during UST, does not show a spectacular shortening of the decay time, evidenced by triangles, circles and squares in Fig. 4(b). This is suggestive of the fact that UST is not perceived as purely thermal process.

Another unique feature of the ultrasound treatment is the significant increase in the forward current at $V \leq 0.25$ V (squares in Fig. 3). This can be readily understood in terms of the decreasing value of $C_{(1)}$ in (7) revealing a decrease in the Schottky barrier height φ_b.

Weighing the results given above, the following scenario describing ultrasound treatments may be applicable. It has been evidenced previously by several authors that the above-barrier defect displacements become feasible with UST [9], [28]–[30]. As evidenced by our thermal annealing measurement, the dominant irradiation-induced defect within the bulk of the structure is the E center. Therefore, the lifetime enhancement in Fig. 4(a) and the subsidiary effects of UST on the $I-V$ characteristics (triangles and squares in Fig. 3) can be understood at least in general terms as due to release of vacancies from the E-centers and their subsequent trapping at defect sinks. Based on the above evidence, it can be proposed that the dominant defects following UST are V and P, the former being locked to electrically inactive configurations at the Si-SiO_2 interface.

This leads to an enhanced density D_S of the interface states in (9) resulting in a decreasing Schottky barrier height. If D_S is high enough, the Bardeen's Fermi level pinning model is applicable and [24]

$$\varphi_{bB} = \left(\frac{E_{gap}}{e} - \Phi_0\right) - \Delta\Phi, \tag{15}$$

where $e\Phi_0$ is the energy level coincident with the Fermi level before the MOS contact was formed and $\Delta\Phi$ is the lowering of the Schottky barrier due to the image force. On the other hand, when D_S is zero, the barrier height is

$$\varphi_{bS} = \Phi_M - \chi - \Delta\Phi, \tag{16}$$

where Φ_M is the metal work function and $e\chi$ is the electron affinity of the semiconductor. In the two extremes, the barrier heights $e\varphi_{bB} = 0.82$ eV and $e\varphi_{bS} = 1.05$ eV are found from (15) and (16), respectively [14], thus illustrating that the increase of the forward currents (triangles and squares in Fig. 3) can indeed be explained in terms of the barrier decrease due to UST.

Note that this picture can be drastically affected by the silicon-oxide interface. Indeed, the activation energies E_A of the forward and reverse currents, obtained from the slope of the Arrhenius plots shown in Fig. 5, are found to be 0.33 eV and 0.68 eV, respectively. The values found in the literature for the activation energy of the oxide- and interface-trap limited performance

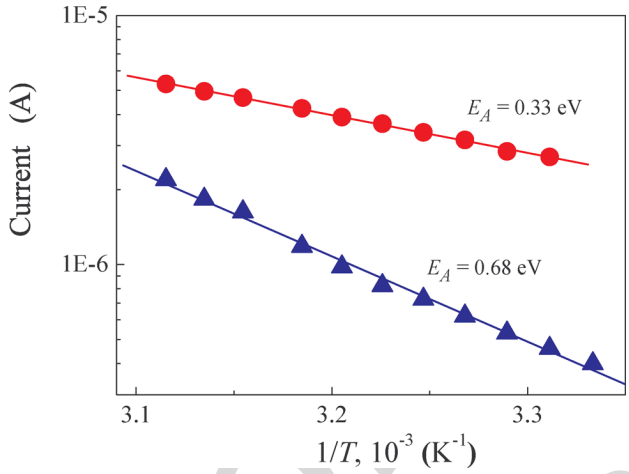

Fig. 5. Forward (circles, $V = 0.6$ V) and reverse (triangles, $V = 2.5$ V) current vs sample temperature. Lines are fitted results to $I \sim \exp(E_A/kT)$, where E_A is the activation energy.

recovery upon thermal annealing cover a broad range [31]–[34]. For example, Stahlbush *et al.* irradiated 1 or 10 Mrad(SiO_2) x-rays and estimated an activation energy of about 0.9 eV for N_{ot} [33]. On the other hand, Lelis *et al.* irradiated 20 krad(SiO_2) x-rays to find out a value of 0.27 eV for N_{ot} [32]. The difference of the experimental activation energies was explained by different gate bias applied during the annealing. Takakura *et al.* reported the activation energy for the trapped-oxide charge (N_{ot}) and Si-SiO_2 interface traps (N_{it}) for the radiation damage of 20 MeV proton irradiated n-MOSFETs to be 0.40 and 0.26 eV, respectively [34]. A direct correlation has been established between the annealing of the oxide-trapped charge and of the E′-centers [9]. This annealing typically occurs in the temperature range between 100 and 300°C. According to Takakura *et al.*, annealed fraction of interface and oxide traps is about 0.9 and 0.97, respectively, at 100°C.

The key Si-SiO_2 interface defect is the P_b-center, corresponding to a silicon dangling bond at the interface, backbonded by three other silicon atoms [9]. The density of the P_b-centers is in good agreement with the density of interface traps. Passivation of these dangling bonds occurs through binding with hydrogen, thus affecting N_{it}. The activation energy of 0.26 eV for the annealing of the interface traps corresponds to the activation energy of about 0.3 eV, attributed to the diffusion of hydrogen in silicon [35], [36]. The annealing of the radiation-induced interface traps is thus governed by the transport of hydrogen towards the interface, where a passivation of the dangling bonds occurs.

The activation energy obtained in this work (0.33 eV) and the γ-irradiation dose used (from 1 to 5 $\times 10^6$ rad) are very close to the ones reported by Parchinskii *et al.* [37]. From these studies, one may conclude that the oxide and interface traps affect the current in our structures.

To understand the effect of UST and to get information about the processes involved, one may consider the potential energy of the defect (cf. vacancies released from the E-centers in Si or hydrogen migrating in SiO_2) as it migrates from the semiconductor into the oxide across the interface; see Fig. 6(a). The

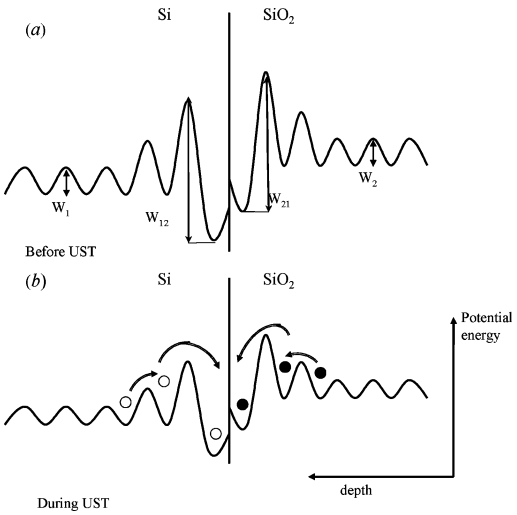

Fig. 6. A schematic picture showing the spatial variation of the potential energy of two defects, in Si and SiO2 layers, as a function of position near the semiconductor-oxide interface. Rf stress lowers the energy barrier for the defects migrating away from the Si and SiO_2 bulk towards the Si-SiO_2 interface [arrows in *(b)*]. The curves in Si and SiO_2 are scaled arbitrarily.

activation energy for the jumps (W_1 and W_2) is smaller than the activation energy for subsequent jumps into the adjacent layer (W_{12} and W_{21}). Therefore, the rf stress used in this work provides a strain-gradient environment in which the defect diffusion takes place. The presence of the stress reduces the energy barrier for the defect jumps towards the interface, as shown by arrows in Fig. 6(b). This may also be understood in terms of the thermodynamic formalism, when the effect of strain on the defect diffusivity D_i is characterized by the change in the activation energy related to the strain tensor ε_{ij} [38]

$$V_{ij}^{*} = kT\frac{\partial lnD_i}{\partial \varepsilon_{ij}}. \tag{17}$$

Of importance is the fact that the strain is alternated in sign, so that the favorable conditions for the defect diffusion towards the interface occur just in a one period of the ultrasonic wave, different in Si and SiO_2 layer.

D. Technological Applications of UST

Understanding and controlling defect diffusion related phenomena are of great interest from scientific and technological aspects. Studying strain effects on the atomic diffusivity, allowing to elucidate atomistic diffusion mechanisms, is also of significant interest in various electronic and renewable energy technologies. This is even more important since, for band-gap engineering purposes, biaxial strain is designed into certain epitaxial semiconductor devices, e.g., heterojunction bipolar transistors for high-power and high-speed applications such as wireless communications. The study of strain effects on diffusion is therefore of crucial importance for improving the stability of these devices.

In this respect, ultrasound treatment is a versatile non-destructive tool for affecting semiconductor heterostructures and devices. The strained and dilated patterns within the structure are spatially and temporally separated, allowing to deliver strain close to the interface and opening new opportunities to controllably affect charge exchange phenomena in the vicinity of the interface. It is of further importance that the strain gradients may be simply varied with frequency, generating a driving force for modification of the electronic parameters in the heterostructure.

In this work, applicability of the technique is demonstrated on the metal-semiconductor Schottky diodes and metal-oxide-semiconductor diodes. These are employed in large area detectors for applications in high energy physics and Schottky barrier devices [39]–[42]. Manipulation of the electrical characteristics of the Schottky barriers is of primary importance for improving radiation hardness of semiconductor devices used in aerospace industry and in advancing the particle detector technology.

A topic of immense interest has been the Schottky diodes for application in power devices and output rectifiers in switching-mode power supplies, and in other high-speed power switching applications, such as motor drives, switching of communication devices, etc. [43].

The observation reported here opens up new possibilities in manipulating electronic properties of metal-semiconductor Schottky diodes and metal-oxide-semiconductor devices. These are heavily influenced by the presence of defects, i.e., higher number of localized electronic states. Ultrasound treatment can help to reduce the number of localized states in a desired area of the device. Hence, the ability to control point defect concentrations in the vicinity of Si-SiO_2 interface is important towards designing superior device performance. With the reported technique, a low-cost integrated device implemented on a piezoelectric substrate traversing acoustic waves (cf. Fig. 1) could be introduced, in which strain fields at the interface are imposed and controlled by an rf voltage applied to the substrate.

IV. Conclusions

A partial recovery of the current-voltage characteristics and photocurrent transient decays are achieved in γ-irradiated silicon by using a room-temperature ultrasonic treatment. A detailed analysis of the $I-V$ characteristics in the metal-silicon structures before and after UST is performed. It is shown that roughly 30% of the irradiation-damaged forward and reverse currents and carrier lifetime could effectively be recovered. The effect can be related to a nearly room-temperature annealing of radiation defects in the ultrasound stress fields, and the release of vacancies from the E-centers with their subsequent trapping at the Si-SiO_2 interface is particularly envisaged.

References

[1] C. Leroy and P.-G. Rancoita, "Particle interaction and displacement damage in silicon devices operated in radiation environments," *Rep. Prog. Phys.*, vol. 70, pp. 493–625, Apr. 2007.

[2] S. Karatas, A. Turut, and S. Altindal, "The timing performance of a two-dimensional position-sensitive silicon detector," *Nucl. Instrum. Methods Phys. Res A*, vol. 555, pp. 260–266, Dec. 2005.

[3] P. Jayavel, M. Udhayasankar, J. Kumar, K. Asokan, and D. Kanjilal, "Electrical characterization of high energy ^{12}C irradiated Au/n-GaAs Schottky Barrier Diodes," *Nucl. Instrum. Methods Phys. Res B*, vol. B156, pp. 110–115, Jul. 1999.

[4] R. C. Newman, "Defects in silicon," *Rep. Prog. Phys.*, vol. 45, pp. 1163–1210, Oct. 1982.

[5] R. A. B. Devine, "The structure of SiO_2, its defects and radiation hardness," *IEEE Trans. Nucl. Sci.*, vol. 41, no. 3, pp. 452–459, Jun. 1994.

[6] G. Niu, G. Banerjee, J. D. Cressler, J. M. Roldan, S. D. Clark, and D. C. Ahlgren, "Electrical probing of surface and bulk traps in proton-irradiated gate-assisted lateral PNP transistors," *IEEE Trans. Nucl. Sci.*, vol. 45, no. 6, pp. 2361–2365, Dec. 1998.

[7] E. H. Nicollian and J. R. Brews, *MOS Physics and Technology*. NewYork: Wiley, 1982.

[8] J. L. Cantin, H. J. Von Bardeleben, and J. L. Autran, "Irradiation effects in ultra thin Si/SiO_2 structures," *IEEE Trans. Nucl. Sci.*, vol. 45, no. 3, pp. 1407–1411, Jun. 1998.

[9] P. M. Lenahan and J. F. Conley Jr., "What can electron paramagnetic resonance tell us about the Si/SiO_2 system," *J. Vac. Sci. Technol. B*, vol. 16, pp. 2134–2153, Jul. 1998.

[10] A. Aassime, G. J. Sarrabayrouse, G. Salace, and C. Petit, "Irradiation effects on the high field behaviour of very thin silica layers," *Solid State Electron.*, vol. 41, pp. 945–949, Jul. 1997.

[11] R. Korde, J. S. Cable, and L. R. Canfield, "One gigarad passivating nitrided oxides for 100% internal quantum efficiency silicon photodiodes," *IEEE Trans. Nucl. Sci.*, vol. 40, no. 6, pp. 1655–1659, Dec. 1993.

[12] D. Schroder and J. F. Babcock, "Negative bias temperature instability: Road to cross in deep sub micron silicon semiconductor manufacturing," *J. Appl. Phys.*, vol. 94, pp. 1–18, Jul. 2003.

[13] D. Esseni, J. D. Bude, and L. Selmi, "On interface and oxide degradation in VLSI MOSFETs – Part I: Deuterium effect in CHE stress regime," *IEEE Trans. Electron Devices*, vol. 49, pp. 247–253, Feb. 2002.

[14] S. Mahapatra, D. Saha, D. Varghese, and P. B. Kumar, "On the generation and recovery of interface traps in MOSFETs subjected to NBTI, FN, and HCI stress," *IEEE Trans. Electron Devices*, vol. 53, pp. 1583–1592, Jul. 2006.

[15] I. V. Ostrovskii, O. A. Korotchenkov, and V. A. Lysykh, "Ultrasonic annealing of point defects in solids," *Sov. Phys. Solid State*, vol. 29, pp. 1239–1240, Jul. 1987.

[16] A. A. Podolyan and V. I. Khivrich, "Room-temperature ultrasonic annealing of radiation defects in silicon," *Tech. Phys. Lett.*, vol. 31, pp. 408–410, May 2005.

[17] N. A. Guseynov, Y. M. Olikh, and S. G. Askerov, "Ultrasonic treatment restores the photoelectric parameters of silicon solar cells degraded under the action of ^{60}Co gamma radiation," *Tech. Phys. Lett.*, vol. 33, pp. 18–21, Jan. 2007.

[18] O. Y. Olikh and T. N. Pinchuk, "Acoustic wave corrected current-voltage characteristics of GaAs-based structures with Schottky contacts," *Tech. Phys. Lett.*, vol. 32, pp. 517–519, Jun. 2006.

[19] S. Ostapenko, N. E. Korsunskaya, and M. K. Sheinkman, "Ultrasound stimulated defect reactions in semiconductors," *Solid State Phenom.*, vol. 85-86, pp. 317–336, 2002.

[20] S. Ostapenko, L. Jastrzebski, J. Lagowski, and R. K. Smeltzer, "Enhanced hydrogenation in polycrystalline silicon thin films using low-temperature ultrasound treatment," *Appl. Phys. Lett.*, vol. 68, pp. 2873–2875, May 1996.

[21] H. Kobayashi, T. Ishida, Y. Nakato, and H. Mori, "Mechanism of carrier transport through a silicon-oxide layer for indium-tin-oxide/silicon-oxide/silicon solar cells," *J. Appl. Phys.*, vol. 78, pp. 3931–3939, Sep. 1995.

[22] S. Biswas and A. Mansingh, "Influence of surface states on current-voltage characteristics of M-I-pSi solar cells," *J. Phys. D, Appl. Phys.*, vol. 25, pp. 100–105, Jan. 1992.

[23] A. Olbrich, B. Ebersberger, and C. Boit, "Conducting atomic force microscopy for nanoscale electrical characterization of thin SiO_2," *Appl. Phys. Lett.*, vol. 73, pp. 3114–3116, Nov. 1998.

[24] S. M. Sze, *Semiconductor Devices, Physics and Technology*. New York: Wiley, 1985.

[25] J. P. McKelvey and R. L. Longini, "Volume and surface recombination rates for injected carriers in germanium," *J. Appl. Phys.*, vol. 25, pp. 634–641, May 1954.

[26] M. Hirata and H. J. Saito, "Effect of impurities on the annealing behavior of irradiated silicon," *J. Appl. Phys.*, vol. 38, pp. 2433–2438, May 1967.

[27] L. A. Kazakevich and P. F. Lugakov, "The effect of dislocations on the radiation defect annealing processes in silicon," *Phys. Stat. Sol. (a)*, vol. 74, pp. 113–122, 1982.

[28] I. V. Ostrovskii, O. A. Korotchenkov, T. Goto, and H. G. Grimmeiss, "Sonoluminescence and acoustically driven optical phenomena in solids and solid-gas interfaces," *Phys. Rep.*, vol. 311, pp. 1–46, Jan. 1999.

[29] Y. M. Olikh, M. D. Tymochko, and A. P. Dolgolenko, "Acoustic-wave-stimulated transformations of radiation defects in γ-irradiated n-type silicon crystals," *Tech. Phys. Lett.*, vol. 32, pp. 586–589, Jul. 2006.

[30] O. Y. Olikh and I. V. Ostrovskii, "Ultrasound-stimulated increase in the electron diffusion length in p-Si crystals," *Phys. Solid State*, vol. 44, pp. 1249–1253, Jul. 2002.

[31] F. Saigne, L. Dusseau, J. Fesquet, J. Gasiot, R. Ecoffet, R. D. Schrimpf, and K. F. Galloway, "Experimental procedure to predict the competition between the degradation induced by irradiation and thermal annealing of oxide trapped charge in MOSFETs," *IEEE Trans. Nucl. Sci.*, vol. 47, no. 6, pp. 2329–2333, Dec. 2000.

[32] A. J. Lelis, T. R. Oldham, H. E. Boesch, Jr, and F. B. McLean, "The nature of the trapped hole annealing process," *IEEE Trans. Nucl. Sci.*, vol. 36, no. 6, pp. 1808–1815, Dec. 1989.

[33] R. E. Stahlbush, A. H. Edwards, D. L. Griscom, and B. J. Mrstik, "Post-irradiation cracking of H_2 and formation of interface states in irradiated metal-oxide-semiconductor field-effect transistors," *J. Appl. Phys.*, vol. 73, pp. 658–667, Jan. 1993.

[34] K. Takakura, H. Ohyama, A. Ueda, M. Nakabayashi, K. Hayama, K. Kobayashi, E. Simoen, A. Mercha, and C. Claeys, "Recovery behaviour resulting from thermal annealing in n-MOSFETs irradiated by 20 MeV protons," *Semicond. Sci. Technol.*, vol. 18, pp. 506–511, Jun. 2003.

[35] D. L. Griscom, "Thermal bleaching of x-ray-induced defect centers in high purity fused silica by diffusion of radiolytic molecular hydrogen," *J. Non-Cryst. Solids*, vol. 68, pp. 301–325, Nov. 1984.

[36] H. Wurzer, R. Mahnkopf, and H. Klose, "Annealing of degraded npn-transistors-mechanisms and modeling," *IEEE Trans. Electron Devices*, vol. 41, pp. 533–538, Apr. 1994.

[37] P. B. Parchinskii, S. I. Vlasov, and A. A. Nasirov, "The effect of γ-ray radiation on the characteristics of the interface between silicon and lead-borosilicate glass," *Semicond.s*, vol. 38, pp. 1304–1307, Nov. 2004.

[38] M. J. Aziz, "Stress effects on defects and dopant diffusion in Si," *Mater. Sci. Semicond. Process.*, vol. 4, pp. 397–403, Oct. 2001.

[39] E. Fretwurst, H. Herdan, G. Lindstrom, U. Pein, M. Rollwagen, H. Schatz, P. Thomsen, and R. Wunstorf, "Silicon detector developments for calorimetry: Technology and radiation damage," *Nucl. Instrum. Methods Phys. Res A*, vol. A288, pp. 1–12, Mar. 1990.

[40] E. Fretwurst, R. Grube, G. Lindstrom, and J. Nagel, "Development of large area silicon detectors: Special properties and radiation stability," *Nucl. Instrum. Methods Phys. Res A*, vol. A253, pp. 467–477, Jan. 1987.

[41] G. Lutz, *Semiconductor Radiation Detectors: Device Physics*. Berlin, Germany: Springer, 2007.

[42] M. Moll aus Ratzeburg, "Radiation Damage in Silicon Particle Detector-Microscopic Defects or Macroscopic Properties," Ph.D. dissertation, Dept. Elect. Eng., Harvard Univ., Cambridge, MA, 1999.

[43] K. K. Ng, *Complete Guide to Semiconductor Devices*. New York: McGraw-Hill, 1995.

Ultrasonically Recovered Performance of γ-Irradiated Metal-Silicon Structures

Alla M. Gorb, Oleg A. Korotchenkov, Oleg Ya. Olikh, and Artem O. Podolian

***Abstract*—The MHz-frequency ultrasound treatment is shown to offer a recovery tool in the current-voltage ($I-V$) characteristics of the γ-irradiated metal-silicon structures. Experimental observations of the ultrasound treatment effect on the carrier transport and photocurrent transient parameters are highlighted. It is shown that up to 30% of the Schottky diode currents and free carrier lifetimes worsen by the irradiation could be recovered in the stress field of ultrasound. The likely scenario behind the treatment effect is outlined, implying the involvement of the vacancies released from the E-centers and subsequently trapped at the Si-SiO_2 interface. It is shown that the technique enables near-room temperature modification of electronic properties of metal-semiconductor Schottky diodes and metal-oxide-semiconductor devices. The density of the electrically active bulk and interface traps can be controllably tuned using this technique. Potential relevance of the processing approach in the context of applications in electronics and detector technologies is pointed out.**

***Index Terms*—Defects, lifetime, radiation, silicon, ultrasound.**

I. Introduction

SILICON is widely used in radiation detectors and electronic devices, and numerous fields of application imply adverse radiation environments that may affect the operation of the devices [1]. Metal-semiconductor Schottky diodes and metal-oxide-semiconductor (MOS) diodes are particularly sensitive to high-level radiations, e.g., to ^{60}Co γ-rays [2], [3]. The formation of lattice defects in the form of vacancies, defect clusters and dislocation loops near the metal-semiconductor interface caused by the irradiation is very harmful for device performance since these defects can act as recombination and trapping centers for charge carriers. Therefore, it is of special interest to develop reliable techniques capable of reducing the number of the electrically active damage defect centers introduced by irradiation. Elevated temperatures are commonly employed in the defect annealing techniques, which inherently pose serious problems of generating thermal donor centers (see [4] and references therein), contaminating a semiconductor in the metal-semiconductor structure due to diffusion of the metal contact material, etc.

Numerous defects located in the bulk and at the Si-SiO_2 interface most relevant for device reliability are the ones which are electrically active, capable of trapping or exchanging charges. Thus, neutral defects are hazardous as they can trap charge during the device working cycle, leading to an accelerating aging. On the other hand, charged defects in the oxide bulk or at the Si-SiO_2 interface influence metal-oxide-semiconductor field-effect transistor (MOSFET) device performance such as threshold voltage of the drain current in the ohmic regime [5], [6]. It is well known that the oxide traps (N_{ot}) and Si-SiO_2 interface traps (N_{it}) are dominant for the degradation of the current-voltage ($I-V$) characteristics in irradiated MOSFETs. Exposure of MOS capacitors to ionizing radiation generates positive charge in the oxide layer and E$'$ centers, resulting from an oxygen vacancy in SiO_2 [7]–[9]. The positive charge can be removed by low-temperature (< 400°C) thermal annealing. It is well known, that nuclear radiation also produces neutral electron traps [10], which cannot be removed by the same annealing. Controlling N_{it} provides a useful way to reduce the harmful effects of lifetime and quantum efficiency degradation in silicon photodiodes [11].

Interface-trap generation is also an important reliability concern in MOSFETs subjected to a negative bias temperature instability, Fowler-Nordheim, and hot-carrier injection stress [12]–[14]. It was reported that the mechanism of N_{it} generation during stress and any recovery of N_{it} after stress must be properly understood for accurate prediction of device lifetime under actual operating conditions.

The treatment of Si with ultrasound (ultrasound treatment, UST) was shown to offer a nearly room-temperature annealing of radiation defects [15]–[18] paving an alternative way to improve the performance of silicon-based devices for particle physics experiments, nuclear medicine and space. A lot of effort has been put into the exploitation of the UST technique in order to engineer and to recover defect-related electronic parameters of silicon [19], [20].

The ultrasound treatment utilized in this work was purpose-built to facilitate the UST concept as a recovery tool in the current-voltage characteristics of the γ-irradiated metal-silicon structures. The next purpose of this work was to introduce the relevant mechanism driving the observed evolution of the $I-V$ characteristics. Understanding of UST effects on irradiated metal-silicon structures would have an impact on the design of the diode devices allowing the development of a specific method for an enhanced radiation stability of these types of semiconductor devices.

II. Experimental

EXPERIMENTS were performed on n-type (111)-oriented crystalline float-zone Si with residual boron (B) impurity concentration of about 10^{12} cm^{-3} and doping phosphorus (P) impurity concentration of 2×10^{12} cm^{-3}. The corresponding

Manuscript received September 07, 2009; revised February 12, 2010; accepted March 05, 2010. Date of current version June 16, 2010. This work was supported in part by the Ministry of Education and Science of Ukraine.

The authors are with the Department of Physics, Taras Shevchenko Kyiv National University, Kyiv 01601, Ukraine (e-mail: g_alla@ukr.net).

Color versions of one or more of the figures in this paper are available online at http://ieeexplore.ieee.org.

Digital Object Identifier 10.1109/TNS.2010.2047655

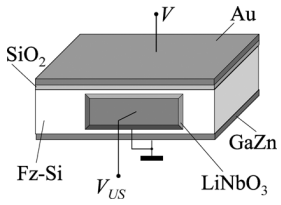

Fig. 1. Schematics of the investigated structure.

resistivity is 4 $\mathrm{k\Omega \cdot cm}$. A bulk silicon material was divided into several rectangular-shaped samples of approximately $1 \times 5 \times 10\ \mathrm{mm^3}$. One of the samples was used as the reference materials, the other ones were γ-irradiated (^{60}Co source) at nominal room temperature to the dose ranged from 5×10^6 to 5×10^7 rad. The resulting conductivity of the samples was reduced to about 0.5 of the initial value. They were found to remain n-type at all irradiation doses used.

The sample geometry is sketched Fig. 1. The Schottky barrier structures, used in the current-voltage measurements, were prepared by chemical etching of the upper Si surfaces using HF-$\mathrm{HNO_3}$-$\mathrm{CH_3COOH}$ solutions (HF: $\mathrm{HNO_3}$: $\mathrm{CH_3COOH} = 3:5:3$), followed by the surface oxidation due to the exposure to ambient air for 24 hours and the Au vacuum evaporation. GaZn-eutectic Ohmic contacts were rubbed on the bottom surfaces of the samples. A metal-oxide-semiconductor (MOS) device was consequently formed. For the photocurrent (PC) decay measurements, GaZn Ohmic contacts were rubbed on the top and bottom contact layers. The area of the upper contact was $\mathrm{A} \approx 50\ \mathrm{mm^2}$ in all cases.

In this work, ultrasound treatment techniques were used to recover defect-related electronic parameters of the irradiated samples. This was done by attaching the $\mathrm{LiNbO_3}$ piezoelectric transducer to one side of the sample, as shown in Fig. 1. An epoxy glue was used as the bonding medium, providing the rigid coupling of the transducer to the sample. The thickness resonant frequency (f) of the transducers was 4 MHz. A radio-frequency (rf) voltage supplied from a generator drives the transducer, resulting in vibrations of the coupled transducer-sample system. The rf strain is then produced in the semiconductor allowing to mechanically modify the electronic properties of the material.

The density of acoustic energy flux (W_{US}) in Si was estimated by neglecting the mechanical loses in the transducers, $W_{US} = V_{US}^2/R_a$, with V_{US} the rf voltage amplitude applied to the transducer and R_a the resistance of an acoustic irradiation. The value of R_a can be expressed as

$$R_a = \frac{1}{8fK^2C_t} \cdot \frac{Z_s}{Z_t}, \tag{1}$$

where K is the coefficient of electro-mechanical coupling of the transducer, C_t is its capacitance, Z_s and Z_t are the impedance of the sample and the transducer, respectively. Data are given below for $W_{US} \approx 2\ \mathrm{W/cm^2}$, yielding the strain amplitude inside the sample of about 10^{-5}.

The sample temperature was measured with a copper-constantan thermocouple directly attached to the sample surface. Ultrasonic treatment was carried out by a series of consecutive loading-unloading cycles, 30 min each. The sample surface temperature raise did not exceed 350 K at the greatest W_{US} used over the course of the loading cycle.

The characteristics of the Au/Si Schottky barrier diode, after γ-irradiation and after UST, were investigated using an $I - V$ measurement technique. For this purpose, computer-driven system based on the analog-to-digital converter ADA-1282 was used. This setup allows to measure forward and reverse bias $I - V$ characteristics for the current varied in the range from $3 \cdot 10^{-10}$ to 10^{-3} A with a voltage step of 0.01 V.

In order to relate the observed $I - V$ changes to defect annealing processes, the photocurrent transient decays were additionally studied before and after ultrasonic treatments. These were taken using a pump pulse generated by a 1.06-μm light-emitting diode (LED) with a half-width of 50 nm. The LED beam that excites the sample was expanded to achieve nominally uniform illumination on the sample surface. The LED was controlled by the external bias in the form of square-function pulse. Light pulse lengths of 100 μs were used, with rise and fall times of ≈ 1.2 μs. The LED pulse sequence had a period of about 50 ms, which was substantially greater than the PC decay time. The background noise level was obtained by averaging the decay signal in the relaxed transient range. The light pulse intensity was controlled so that the low-level injection conditions were satisfied (the injected carrier concentration was 1% of its steady value). Decay transients were stored in the computer memory using an analog-to-digital converter with a resolution of 2 μs. RC time constants were observed to be less than 100 ns, which was much smaller than the time scales of interest.

The transient PC is due to mobile excess electrons and holes, generated by the light-induced band-to-band transitions. If the decay behavior of electrons and holes is identical, the excess densities of electrons and holes are equal at every instant. This condition is usually satisfied in the low-level carrier injection range, when the charge carrier transport is controlled by the minority carriers. For a uniform distribution of excess carriers the transient photoconductivity $\Delta\sigma(t) = \Delta n(t)(\mu_n + \mu_p)e$, where $\Delta n(t)$ is the excess density of minority carriers, μ_n and μ_p are the mobility of electrons and holes, respectively, and e is the electron charge. A relaxation (decay) time $\tau(t)$ for the excess minority carrier density can be defined as

$$\frac{1}{\tau(t)} = -\frac{1}{\triangle n(t)} \frac{\partial \triangle n(t)}{\partial t}, \tag{2}$$

which is also the decay time of the photoconductivity.

The heat treatments were carried out by isochronal anneals at temperatures ranging between 350 and 530 K in a quartz-tube furnace under ambient conditions.

III. Results and Discussion

A. A Brief Introduction to Carrier Transport Mechanisms

Due to the presence of surface or interface states in the band gap of a semiconductor, the Fermi level at the surface (or interface) may have a different position with respect to the band edges than in the bulk. At thermal equilibrium, the Fermi level is

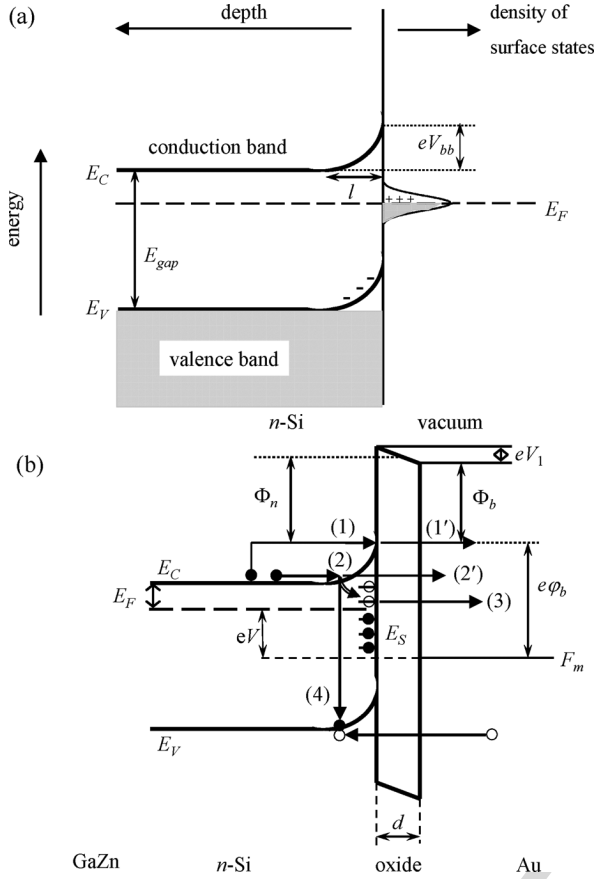

Fig. 2. Band diagrams of MOS devices: (a) in equilibrium, in the absence of the insulating layer, (b) at externally applied voltage V, with the oxide layer of the thickness of d. The diagrams illustrate the band bending V_{bb} in the subsurface region of an n-doped semiconductor which have surface states within the band gap. Φ_b is the Schottky barrier height, Φ_n is the mean barrier height, E_F and F_m are the Fermi levels in Si and Au, respectively, $\Phi_n = \Phi_b + eV_1/2$. Each of the horizontal lines E_S in (b) represents an interface trap. It is either occupied by an electron (solid circle) or occupied by a hole (open circle). Arrows (1)-(4) represent the main carrier transport mechanisms discussed in the text.

constant throughout the crystal, thus yielding a charge transfer between surface and bulk. Consequently, the surface is charged with the charge value which is balanced by an opposite space charge in a layer underneath the surface. Assume that the energetic position and occupancy of the surface states within the band gap is such that the charge transfer depletes the subsurface layer of majority carriers. Then the charge distribution produces an electric field within the space charge region and a corresponding band bending, which can be obtained from Poisson's equation and is shown in Fig. 2. The thickness l of the depletion layer is

$$l = \sqrt{\frac{2\varepsilon\varepsilon_0 V_{bb}}{eN_D}}, \tag{3}$$

where V_{bb} is the magnitude of the band bending, N_D is the bulk dopant concentration, ε is the dielectric constant and ε_0 is the dielectric constant of free space.

The density of a dark current I, flowing between metal and semiconductor, in the n-type semiconductor-based MOS device under a forward bias is as follows [21]

$$I = CP_t(e^{eV_2/nkT} - 1), \tag{4}$$

where V_2 is the voltage drop across the space-charge (depletion) region of the semiconductor, n is the ideality factor, k is the Boltzman constant, T is the temperature, P_t is the carrier transfer probability through the insulating layer, and C is a coefficient.

Furthermore, in the more general case, the current is limited by the series resistance, which is due to the contact resistance between the metal and the semiconductor, the resistance of the thin insulating layer, the resistance of the semiconductor or the resistance of the connecting wires. Since, in high-resistivity Si, the resistance of the semiconductor R_S cannot be neglected, the bias voltage applied to the top metal electrode (cf. Fig. 1) V is

$$V = V_1 + V_2 + IR_S, \tag{5}$$

where V_1 is the voltage drop across the insulating oxide layer, IR_S is the voltage drop across the quasi-neutral region of the semiconductor of width l in Fig. 2(a).

In case of the quantum mechanical tunneling through the insulating layer [processes (1') and (3) in Fig. 2(b)] the probability P_t is

$$P_t = e^{-t\sqrt{\Phi_n}d}, \tag{6}$$

where t is the tunneling constant which is $t = \sqrt{2m^*\hbar}$, m^* is the effective electron mass in SiO_2 ($\sim 0.5\ m_0$), m_0 is the free electron mass, and $\hbar$ is the Planck constant. Overcoming the Schottky barrier by process (1) in Fig. 2(b) can be described in the thermionic emission model, and the coefficient C is given by

$$C = C_{(1)} = A^*T^2e^{-e\varphi_b/kT}, \tag{7}$$

where φ_b is the Schottky barrier height in the semiconductor for the MOS region and A^* is the modified Richardson constant. Then the total current transmitted through the processes (1) and (1') is

$$I_{(1)} = A^*T^2e^{-e\varphi_b/kT}e^{-t\sqrt{\Phi_n}d}(e^{eV_2/nkT} - 1). \tag{8}$$

The ideality factor $n = 1$ if the recombination-generation current developed due to band-to-band recombination/generation [process (4) in Fig. 2(b)] is unimportant, and $1 < n < 2$ otherwise.

Since the doping concentration in our samples is low ($\approx 10^{12}\ \mathrm{cm}^{-3}$), the width of the depleted region l, obtained from (1), is large enough, of about 20 μm. Then there is hardly the Schottky barrier and the insulating layer to tunnel through, and the migration pathway sketched by process (2) in Fig. 2(b)

is likely to be avoided by the carrier in favor of an easier route (1)-(1'). The experimentally observed current may therefore be dominated by process (1)-(1') and the $I_{(2)}$ component can be neglected.

If pathway (1)-(1') in Fig. 2(b) is the dominant process, the mean barrier height Φ_n at the silicon-oxide interface can be calculated from the slope of the semilogarithmic $I-d$ plot. If $V_1 \ll V_2$, the logarithmic plot of $I/[1-\exp(-eV/nkT)]$ against V is linear. In this case, $A^*T^2 \cdot e^{-e\varphi_b/kT}$ can be obtained from the I-axis intercept at zero V, and from this the barrier height φ_b can be derived.

The effect of tunnelling through the interface states E_S [process (3) in Fig. 2(b)] can be achieved by introducing the density D_S of the interface states, which are evenly distributed in the energy range ΔE_S, the capture cross-section σ_{St} of the interface states for tunnelling, and the occupational probability f_S of the interface states. In this process, the electrons, captured at the interface states [curved arrow in Fig. 2(b)], tunnel from these states to vacant states in the metal (Au). A backward tunnelling of electrons from the metal to the interface states should also be taken into account. Then the current is [22]

$$I_{(3)} = eD_S F_S \sigma_{St} \upsilon_m g(E_S) \Delta E_S \cdot e^{-t\sqrt{\Phi_S}d} \times (1 - e^{-eV_1/kt}), \tag{9}$$

where υ_m is the thermal velocity of electrons in the metal, $g(E_S)$ is the density of states in the metal at the energy of E_S, and Φ_S is the barrier height for electrons captured at the interface states.

Obviously, in the general case, the current through the MOS device is equal to the algebraic sum of $I_{(1)}$, $I_{(2)}$ and the current $I_{(3)}$ due to tunnelling via the interface states. This, of course, complicates the analysis of the measured $I-V$ curves.

B. Change in the Carrier Transport and Photocurrent Transient Parameters of Irradiated MOS Structures

Fig. 3 shows the semilogarithmic plots of the forward- and reverse-bias $I-V$ characteristics of one of the MOS structures, taken before and after γ-irradiation (solid and open circles, respectively). It is seen that the plot taken before γ-irradiation consists of a good linear range with a well-defined intermediate-bias region followed by the current saturation. In contrast, the intermediate-bias region with different slopes is achieved in the irradiated sample at much lower voltages, thus making a linear range less pronounced and decreasing substantially the value of the saturation current.

These experimental results can be interpreted in the light of the above models. The forward $I-V$ curves shown in Fig. 3 can be analyzed using the Schottky barrier thermionic emission model, so that

$$I = I_S(e^{e(V-IR_S)/nkT} - 1), \tag{10}$$

which is derived from (8) under the simplifying assumption that $V_1 \ll V_2$ and introducing the saturation current $I_S = AA^*T^2 e^{-e\varphi_b/kT} e^{-t\sqrt{\Phi_n}d}$.

The results of simulations shown by solid curves in the inset of Fig. 3 reveal a very good correspondence between the

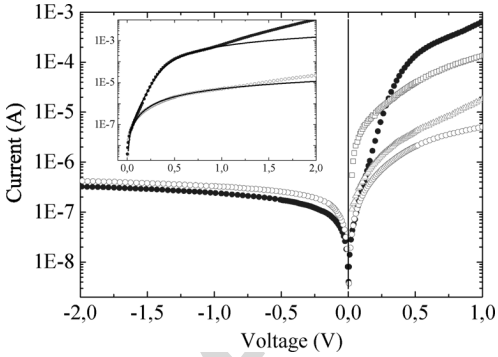

Fig. 3. The reverse and forward $I-V$ curves of the Au-SiO_2-Si Schottky barrier structure taken before (solid circles) and after (open circles) γ-irradiation. $T = 295$ K. Inset enlarges the forward bias region, the solid lines are the fitting curves calculated by using (9) with $I_S = 5 \times 10^{-8}$ A, $R_S = 10^3\ \Omega$ (upper curve) and $1.5 \times 10^5\ \Omega$ (lower curve). Effect of ultrasound treatment is illustrated by triangles (30-min UST) and squares (60-min).

measured and computed $I-V$ characteristics at $V \leq 1$ V, with the discrepancies which arise at greater voltages. Within a schematic picture shown in Fig. 2(b) this result may be interpreted such that two different processes (1) and (1') are present in the electron pathway. Indeed, the current saturation is achieved at the condition when the V-dependent resistance of the depleted region approaches the sum of R_S and the resistance of the oxide layer, which is achieved at about 0.4 V in the pre-irradiated sample. Increasing V imposes decreased band bending and width of the depletion region (eV_{bb} and l in Fig. 2(a), respectively), thus enhancing the electron capture probability at the interface states. Then the current through process (3) in Fig. 2(b) turns out to be favorable, which may lead to increased current above ≈ 1 V observed in the inset of Fig. 3.

Furthermore, as the applied voltage V increases above ≈ 1.6 V, the charge density at the interface becomes so high that it leaks through the oxide by Fowler-Nordheim or direct tunneling mechanism, which can be described by [23]

$$I = A\frac{e^3}{16\pi^2\hbar\Phi_n}\frac{m_0}{m^*}\left(\frac{V}{d}\right)^2 \exp\left(-\frac{4\sqrt{2m^*}}{3e\hbar}\frac{d}{V}\Phi_n^{3/2}\right), \tag{11}$$

where A is the tunneling area. It is observed that the Fowler-Nordheim plot of $\ln(I/V^2)$ *vs* $1/V$ clearly exhibits a linear relationship above ≈ 1.6 V. Therefore, the above discrepancies can also be due to electron tunneling at a large bias, which subsequently increases the measured current.

Since γ-irradiation causes the increase in the sample resistance R_S, the saturation condition, $V_2 \approx V_1 + IR_S$, is achieved at a lower voltage V, applied to the structure. This leads to a decrease in the saturation current in the irradiated sample, as observed both experimentally and theoretically in Fig. 3. However, the increase in the fitting value of R_S for the curves shown in the inset of Fig. 3 is substantially greater than the measured resistivity enhancement (about two times greater) observed after irradiation. More detailed understanding of the structural and compositional complexity of oxide layers grown on the irradiated surface seems to be necessary to reveal in order to account

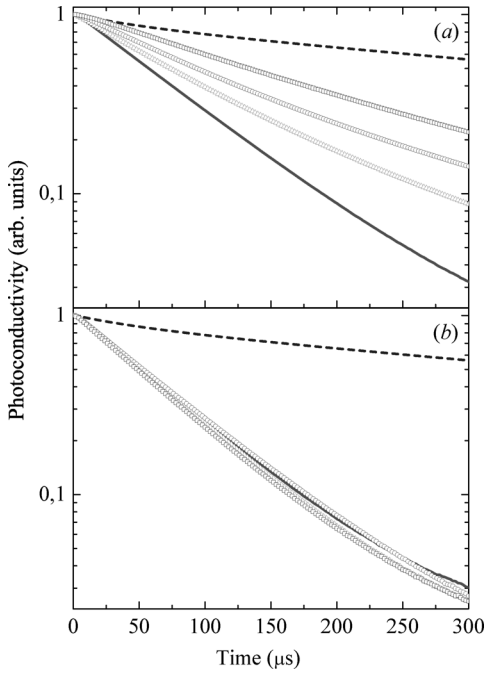

Fig. 4. Photocurrent transient decays taken before (dotted curves) and after (solid curves) γ-irradiation (5×10^6 rad), and after ultrasound *(a)* and thermal *(b)* treatments of the irradiated sample. UST is performed during 60 (triangles), 120 (circles) and 240 (squares) min. Thermal treatment is performed at 360 K during 60 (triangles), 120 (circles) and 240 (squares) min. The surface recombination velocity is kept constant at about $S = 10^3$ cm/s. The carrier lifetime $\tau = 500(1), 77(2), 100(3), 119(4)$ and 177 μs (5).

correctly for an increased resistance of the oxide layer grown on the irradiated surface.

At reverse bias, a square-root dependence $I_R \sim \sqrt{V}$ is observed for $\mathrm{V} > 1$ V, signifying that the generation-recombination process [process (4) in Fig. 2(b)] determines the current mechanism. Indeed, the reverse current is [24]

$$I_R = \frac{eAn_i l}{2\tau}, \tag{12}$$

where n_i is the charge carrier concentration in the intrinsic semiconductor and τ is the free carrier lifetime with respect to recombination and trapping in the depleted region. Since $l \sim \sqrt{V_{bb} + V_2}$, the square-root dependence is expected for the generation-recombination process, which is indeed observed experimentally.

Changes in τ can be obtained from PC decay measurements shown in Fig. 4. The decays are nearly simple exponentials with the measured lifetimes τ, which are effective lifetimes integrating bulk (τ_b) and surface (τ_s) recombination components [25]:

$$\frac{1}{\tau} = \frac{1}{\tau_b} + \frac{1}{\tau_s} = \frac{1}{\tau_b} + \pi^2 D \left(\frac{\xi^2}{l_1^2} + \frac{\eta^2}{l_2^2} + \frac{\zeta^2}{l_3^2} \right), \tag{13}$$

TABLE I
ULTRASOUND MODIFICATION OF THE RECTIFICATION FACTOR OF THE MOS DEVICE TAKEN AT $V = 0.35$ V AND OF THE FREE CARRIER LIFETIME τ OBTAINED FROM THE PHOTOCURRENT DECAY.

Parametr	ST duration (min)		
	0	30	60
k_r	0.3	1.6	85
τ_1/τ_{01}	1	1.2	1.4
τ_2/τ_{02}	1	-	1.3

τ_{01} and τ_1 are the carrier lifetimes in the irradiated and subsequently ultrasound treated structure, respectively, obtained from Eq. (12). τ_2 and τ_{02} are the ones obtained from the photocurrent decays.

where D is the diffusion coefficient of the minority carrier, l_1, l_2 and l_3 are the linear dimensions of the sample, and ξ, η and ζ are determined from the following characteristic equations:

$$cot\left(\frac{\xi\pi}{2}\right) = \frac{\xi\pi D}{Sd_1}, cot\left(\frac{\eta\pi}{2}\right) = \frac{\eta\pi D}{Sd_2}, cot\left(\frac{\zeta\pi}{2}\right) = \frac{\zeta\pi D}{Sd_3} \tag{14}$$

with S the surface recombination velocity. Therefore, if the surface effect is fixed by fixing S the values of τ obtained in Fig. 4 exhibit the bulk lifetimes τ_b.

Irradiation produces a considerable decrease in the carrier lifetime, as evidenced by comparing dotted and solid curves in Fig. 4, which is indicative of enhanced defect concentrations in the structures. The latter is due to the fact that γ-irradiation produces vacancies and self-interstitials, which may combine with impurities to form complexes of defects. These can act as efficient recombination centers yielding the observed shortening of the minority carrier lifetime. The thermal annealing behavior of the lifetime (not shown here) can qualitatively be described as due to at least two types of defects, which anneal by ≈ 150 and 225°C. The former lifetime recovery stage correlates with the E-center (vacancy V trapped at atom P) anneal [26], whereas the latter one would come from the anneal of the divacancy V_2 [27].

Hence there appears to be an interplay between the terms describing the variation of the reverse current in (12). The observed decrease in τ and decrease in the thickness l of the depletion layer with increasing defect concentration in the irradiated structure likely to result in enhanced I_R seen in Fig. 3 (open circles).

C. Ultrasound Treatment Effect on the Carrier Transport and Photocurrent Transient Parameters

The effect of UST on the forward $I - V$ characteristics is shown in Fig. 3 by triangles and squares. The reverse currents are also affected by ultrasound, and the effect on the carrier transport parameters can be explicitly illustrated in terms of the rectification factor k_r of the structure, which is defined as the ratio of the forward and the reverse currents (see Table I).

It turned out that the most essential features of UST are the remarkable increase of the forward currents (triangles and squares in Fig. 3) and of the diode rectification factor (k_r in Table I). The latter is in part due to the increase in τ (data of Table I) and the subsequent decrease in the reverse current, both of which are observed experimentally. The lifetime increase due to UST is exemplified by a slowing down the decay curves shown by triangles, circles and squares in Fig. 4(a). Because the magnitude

of the reverse current is inversely proportional to τ, the current is found to decrease with UST in a way that is prescribed by (12).

Of prime importance is the fact that the sample exposure to thermal treatments at 360 K, which is slightly greater than the highest possible value of the sample temperature during UST, does not show a spectacular shortening of the decay time, evidenced by triangles, circles and squares in Fig. 4(b). This is suggestive of the fact that UST is not perceived as purely thermal process.

Another unique feature of the ultrasound treatment is the significant increase in the forward current at $V \leq 0.25$ V (squares in Fig. 3). This can be readily understood in terms of the decreasing value of $C_{(1)}$ in (7) revealing a decrease in the Schottky barrier height φ_b.

Weighing the results given above, the following scenario describing ultrasound treatments may be applicable. It has been evidenced previously by several authors that the above-barrier defect displacements become feasible with UST [9], [28]–[30]. As evidenced by our thermal annealing measurement, the dominant irradiation-induced defect within the bulk of the structure is the E center. Therefore, the lifetime enhancement in Fig. 4(a) and the subsidiary effects of UST on the $I-V$ characteristics (triangles and squares in Fig. 3) can be understood at least in general terms as due to release of vacancies from the E-centers and their subsequent trapping at defect sinks. Based on the above evidence, it can be proposed that the dominant defects following UST are V and P, the former being locked to electrically inactive configurations at the Si-SiO_2 interface.

This leads to an enhanced density D_S of the interface states in (9) resulting in a decreasing Schottky barrier height. If D_S is high enough, the Bardeen's Fermi level pinning model is applicable and [24]

$$\varphi_{bB} = \left(\frac{E_{gap}}{e} - \Phi_0\right) - \Delta\Phi, \tag{15}$$

where $e\Phi_0$ is the energy level coincident with the Fermi level before the MOS contact was formed and $\Delta\Phi$ is the lowering of the Schottky barrier due to the image force. On the other hand, when D_S is zero, the barrier height is

$$\varphi_{bS} = \Phi_M - \chi - \Delta\Phi, \tag{16}$$

where Φ_M is the metal work function and $e\chi$ is the electron affinity of the semiconductor. In the two extremes, the barrier heights $e\varphi_{bB} = 0.82$ eV and $e\varphi_{bS} = 1.05$ eV are found from (15) and (16), respectively [14], thus illustrating that the increase of the forward currents (triangles and squares in Fig. 3) can indeed be explained in terms of the barrier decrease due to UST.

Note that this picture can be drastically affected by the silicon-oxide interface. Indeed, the activation energies E_A of the forward and reverse currents, obtained from the slope of the Arrhenius plots shown in Fig. 5, are found to be 0.33 eV and 0.68 eV, respectively. The values found in the literature for the activation energy of the oxide- and interface-trap limited performance

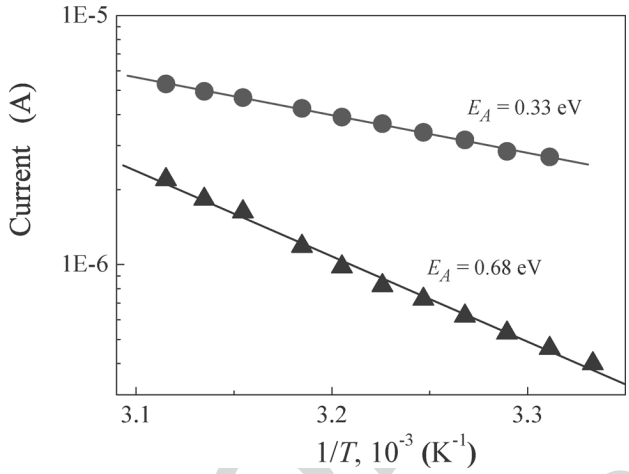

Fig. 5. Forward (circles, $V = 0.6$ V) and reverse (triangles, $V = 2.5$ V) current vs sample temperature. Lines are fitted results to $I \sim \exp(E_A/kT)$, where E_A is the activation energy.

recovery upon thermal annealing cover a broad range [31]–[34]. For example, Stahlbush *et al.* irradiated 1 or 10 Mrad(SiO_2) x-rays and estimated an activation energy of about 0.9 eV for N_{ot} [33]. On the other hand, Lelis *et al.* irradiated 20 krad(SiO_2) x-rays to find out a value of 0.27 eV for N_{ot} [32]. The difference of the experimental activation energies was explained by different gate bias applied during the annealing. Takakura *et al.* reported the activation energy for the trapped-oxide charge (N_{ot}) and Si-SiO_2 interface traps (N_{it}) for the radiation damage of 20 MeV proton irradiated n-MOSFETs to be 0.40 and 0.26 eV, respectively [34]. A direct correlation has been established between the annealing of the oxide-trapped charge and of the E′-centers [9]. This annealing typically occurs in the temperature range between 100 and 300°C. According to Takakura *et al.*, annealed fraction of interface and oxide traps is about 0.9 and 0.97, respectively, at 100°C.

The key Si-SiO_2 interface defect is the P_b-center, corresponding to a silicon dangling bond at the interface, backbonded by three other silicon atoms [9]. The density of the P_b-centers is in good agreement with the density of interface traps. Passivation of these dangling bonds occurs through binding with hydrogen, thus affecting N_{it}. The activation energy of 0.26 eV for the annealing of the interface traps corresponds to the activation energy of about 0.3 eV, attributed to the diffusion of hydrogen in silicon [35], [36]. The annealing of the radiation-induced interface traps is thus governed by the transport of hydrogen towards the interface, where a passivation of the dangling bonds occurs.

The activation energy obtained in this work (0.33 eV) and the γ-irradiation dose used (from 1 to 5 $\times 10^6$ rad) are very close to the ones reported by Parchinskii *et al.* [37]. From these studies, one may conclude that the oxide and interface traps affect the current in our structures.

To understand the effect of UST and to get information about the processes involved, one may consider the potential energy of the defect (cf. vacancies released from the E-centers in Si or hydrogen migrating in SiO_2) as it migrates from the semiconductor into the oxide across the interface; see Fig. 6(a). The

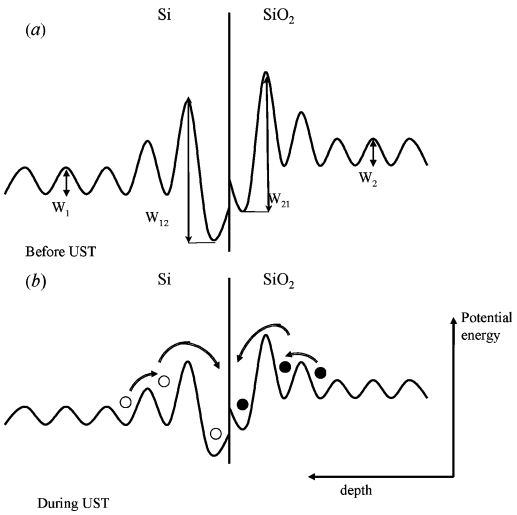

Fig. 6. A schematic picture showing the spatial variation of the potential energy of two defects, in Si and SiO2 layers, as a function of position near the semiconductor-oxide interface. Rf stress lowers the energy barrier for the defects migrating away from the Si and SiO_2 bulk towards the Si-SiO_2 interface [arrows in *(b)*]. The curves in Si and SiO_2 are scaled arbitrarily.

activation energy for the jumps (W_1 and W_2) is smaller than the activation energy for subsequent jumps into the adjacent layer (W_{12} and W_{21}). Therefore, the rf stress used in this work provides a strain-gradient environment in which the defect diffusion takes place. The presence of the stress reduces the energy barrier for the defect jumps towards the interface, as shown by arrows in Fig. 6(b). This may also be understood in terms of the thermodynamic formalism, when the effect of strain on the defect diffusivity D_i is characterized by the change in the activation energy related to the strain tensor ε_{ij} [38]

$$V_{ij}^{*} = kT\frac{\partial lnD_i}{\partial \varepsilon_{ij}}. \tag{17}$$

Of importance is the fact that the strain is alternated in sign, so that the favorable conditions for the defect diffusion towards the interface occur just in a one period of the ultrasonic wave, different in Si and SiO_2 layer.

D. Technological Applications of UST

Understanding and controlling defect diffusion related phenomena are of great interest from scientific and technological aspects. Studying strain effects on the atomic diffusivity, allowing to elucidate atomistic diffusion mechanisms, is also of significant interest in various electronic and renewable energy technologies. This is even more important since, for band-gap engineering purposes, biaxial strain is designed into certain epitaxial semiconductor devices, e.g., heterojunction bipolar transistors for high-power and high-speed applications such as wireless communications. The study of strain effects on diffusion is therefore of crucial importance for improving the stability of these devices.

In this respect, ultrasound treatment is a versatile non-destructive tool for affecting semiconductor heterostructures and devices. The strained and dilated patterns within the structure are spatially and temporally separated, allowing to deliver strain close to the interface and opening new opportunities to controllably affect charge exchange phenomena in the vicinity of the interface. It is of further importance that the strain gradients may be simply varied with frequency, generating a driving force for modification of the electronic parameters in the heterostructure.

In this work, applicability of the technique is demonstrated on the metal-semiconductor Schottky diodes and metal-oxide-semiconductor diodes. These are employed in large area detectors for applications in high energy physics and Schottky barrier devices [39]–[42]. Manipulation of the electrical characteristics of the Schottky barriers is of primary importance for improving radiation hardness of semiconductor devices used in aerospace industry and in advancing the particle detector technology.

A topic of immense interest has been the Schottky diodes for application in power devices and output rectifiers in switching-mode power supplies, and in other high-speed power switching applications, such as motor drives, switching of communication devices, etc. [43].

The observation reported here opens up new possibilities in manipulating electronic properties of metal-semiconductor Schottky diodes and metal-oxide-semiconductor devices. These are heavily influenced by the presence of defects, i.e., higher number of localized electronic states. Ultrasound treatment can help to reduce the number of localized states in a desired area of the device. Hence, the ability to control point defect concentrations in the vicinity of Si-SiO_2 interface is important towards designing superior device performance. With the reported technique, a low-cost integrated device implemented on a piezoelectric substrate traversing acoustic waves (cf. Fig. 1) could be introduced, in which strain fields at the interface are imposed and controlled by an rf voltage applied to the substrate.

IV. Conclusions

A partial recovery of the current-voltage characteristics and photocurrent transient decays are achieved in γ-irradiated silicon by using a room-temperature ultrasonic treatment. A detailed analysis of the $I-V$ characteristics in the metal-silicon structures before and after UST is performed. It is shown that roughly 30% of the irradiation-damaged forward and reverse currents and carrier lifetime could effectively be recovered. The effect can be related to a nearly room-temperature annealing of radiation defects in the ultrasound stress fields, and the release of vacancies from the E-centers with their subsequent trapping at the Si-SiO_2 interface is particularly envisaged.

References

[1] C. Leroy and P.-G. Rancoita, "Particle interaction and displacement damage in silicon devices operated in radiation environments," *Rep. Prog. Phys.*, vol. 70, pp. 493–625, Apr. 2007.

[2] S. Karatas, A. Turut, and S. Altindal, "The timing performance of a two-dimensional position-sensitive silicon detector," *Nucl. Instrum. Methods Phys. Res A*, vol. 555, pp. 260–266, Dec. 2005.

[3] P. Jayavel, M. Udhayasankar, J. Kumar, K. Asokan, and D. Kanjilal, "Electrical characterization of high energy ^{12}C irradiated Au/n-GaAs Schottky Barrier Diodes," *Nucl. Instrum. Methods Phys. Res B*, vol. B156, pp. 110–115, Jul. 1999.

[4] R. C. Newman, "Defects in silicon," *Rep. Prog. Phys.*, vol. 45, pp. 1163–1210, Oct. 1982.

[5] R. A. B. Devine, "The structure of SiO_2, its defects and radiation hardness," *IEEE Trans. Nucl. Sci.*, vol. 41, no. 3, pp. 452–459, Jun. 1994.

[6] G. Niu, G. Banerjee, J. D. Cressler, J. M. Roldan, S. D. Clark, and D. C. Ahlgren, "Electrical probing of surface and bulk traps in proton-irradiated gate-assisted lateral PNP transistors," *IEEE Trans. Nucl. Sci.*, vol. 45, no. 6, pp. 2361–2365, Dec. 1998.

[7] E. H. Nicollian and J. R. Brews, *MOS Physics and Technology*. NewYork: Wiley, 1982.

[8] J. L. Cantin, H. J. Von Bardeleben, and J. L. Autran, "Irradiation effects in ultra thin Si/SiO_2 structures," *IEEE Trans. Nucl. Sci.*, vol. 45, no. 3, pp. 1407–1411, Jun. 1998.

[9] P. M. Lenahan and J. F. Conley Jr., "What can electron paramagnetic resonance tell us about the Si/SiO_2 system," *J. Vac. Sci. Technol. B*, vol. 16, pp. 2134–2153, Jul. 1998.

[10] A. Aassime, G. J. Sarrabayrouse, G. Salace, and C. Petit, "Irradiation effects on the high field behaviour of very thin silica layers," *Solid State Electron.*, vol. 41, pp. 945–949, Jul. 1997.

[11] R. Korde, J. S. Cable, and L. R. Canfield, "One gigarad passivating nitrided oxides for 100% internal quantum efficiency silicon photodiodes," *IEEE Trans. Nucl. Sci.*, vol. 40, no. 6, pp. 1655–1659, Dec. 1993.

[12] D. Schroder and J. F. Babcock, "Negative bias temperature instability: Road to cross in deep sub micron silicon semiconductor manufacturing," *J. Appl. Phys.*, vol. 94, pp. 1–18, Jul. 2003.

[13] D. Esseni, J. D. Bude, and L. Selmi, "On interface and oxide degradation in VLSI MOSFETs – Part I: Deuterium effect in CHE stress regime," *IEEE Trans. Electron Devices*, vol. 49, pp. 247–253, Feb. 2002.

[14] S. Mahapatra, D. Saha, D. Varghese, and P. B. Kumar, "On the generation and recovery of interface traps in MOSFETs subjected to NBTI, FN, and HCI stress," *IEEE Trans. Electron Devices*, vol. 53, pp. 1583–1592, Jul. 2006.

[15] I. V. Ostrovskii, O. A. Korotchenkov, and V. A. Lysykh, "Ultrasonic annealing of point defects in solids," *Sov. Phys. Solid State*, vol. 29, pp. 1239–1240, Jul. 1987.

[16] A. A. Podolyan and V. I. Khivrich, "Room-temperature ultrasonic annealing of radiation defects in silicon," *Tech. Phys. Lett.*, vol. 31, pp. 408–410, May 2005.

[17] N. A. Guseynov, Y. M. Olikh, and S. G. Askerov, "Ultrasonic treatment restores the photoelectric parameters of silicon solar cells degraded under the action of ^{60}Co gamma radiation," *Tech. Phys. Lett.*, vol. 33, pp. 18–21, Jan. 2007.

[18] O. Y. Olikh and T. N. Pinchuk, "Acoustic wave corrected current-voltage characteristics of GaAs-based structures with Schottky contacts," *Tech. Phys. Lett.*, vol. 32, pp. 517–519, Jun. 2006.

[19] S. Ostapenko, N. E. Korsunskaya, and M. K. Sheinkman, "Ultrasound stimulated defect reactions in semiconductors," *Solid State Phenom.*, vol. 85-86, pp. 317–336, 2002.

[20] S. Ostapenko, L. Jastrzebski, J. Lagowski, and R. K. Smeltzer, "Enhanced hydrogenation in polycrystalline silicon thin films using low-temperature ultrasound treatment," *Appl. Phys. Lett.*, vol. 68, pp. 2873–2875, May 1996.

[21] H. Kobayashi, T. Ishida, Y. Nakato, and H. Mori, "Mechanism of carrier transport through a silicon-oxide layer for indium-tin-oxide/silicon-oxide/silicon solar cells," *J. Appl. Phys.*, vol. 78, pp. 3931–3939, Sep. 1995.

[22] S. Biswas and A. Mansingh, "Influence of surface states on current-voltage characteristics of M-I-pSi solar cells," *J. Phys. D, Appl. Phys.*, vol. 25, pp. 100–105, Jan. 1992.

[23] A. Olbrich, B. Ebersberger, and C. Boit, "Conducting atomic force microscopy for nanoscale electrical characterization of thin SiO_2," *Appl. Phys. Lett.*, vol. 73, pp. 3114–3116, Nov. 1998.

[24] S. M. Sze, *Semiconductor Devices, Physics and Technology*. New York: Wiley, 1985.

[25] J. P. McKelvey and R. L. Longini, "Volume and surface recombination rates for injected carriers in germanium," *J. Appl. Phys.*, vol. 25, pp. 634–641, May 1954.

[26] M. Hirata and H. J. Saito, "Effect of impurities on the annealing behavior of irradiated silicon," *J. Appl. Phys.*, vol. 38, pp. 2433–2438, May 1967.

[27] L. A. Kazakevich and P. F. Lugakov, "The effect of dislocations on the radiation defect annealing processes in silicon," *Phys. Stat. Sol. (a)*, vol. 74, pp. 113–122, 1982.

[28] I. V. Ostrovskii, O. A. Korotchenkov, T. Goto, and H. G. Grimmeiss, "Sonoluminescence and acoustically driven optical phenomena in solids and solid-gas interfaces," *Phys. Rep.*, vol. 311, pp. 1–46, Jan. 1999.

[29] Y. M. Olikh, M. D. Tymochko, and A. P. Dolgolenko, "Acoustic-wave-stimulated transformations of radiation defects in γ-irradiated n-type silicon crystals," *Tech. Phys. Lett.*, vol. 32, pp. 586–589, Jul. 2006.

[30] O. Y. Olikh and I. V. Ostrovskii, "Ultrasound-stimulated increase in the electron diffusion length in p-Si crystals," *Phys. Solid State*, vol. 44, pp. 1249–1253, Jul. 2002.

[31] F. Saigne, L. Dusseau, J. Fesquet, J. Gasiot, R. Ecoffet, R. D. Schrimpf, and K. F. Galloway, "Experimental procedure to predict the competition between the degradation induced by irradiation and thermal annealing of oxide trapped charge in MOSFETs," *IEEE Trans. Nucl. Sci.*, vol. 47, no. 6, pp. 2329–2333, Dec. 2000.

[32] A. J. Lelis, T. R. Oldham, H. E. Boesch, Jr, and F. B. McLean, "The nature of the trapped hole annealing process," *IEEE Trans. Nucl. Sci.*, vol. 36, no. 6, pp. 1808–1815, Dec. 1989.

[33] R. E. Stahlbush, A. H. Edwards, D. L. Griscom, and B. J. Mrstik, "Post-irradiation cracking of H_2 and formation of interface states in irradiated metal-oxide-semiconductor field-effect transistors," *J. Appl. Phys.*, vol. 73, pp. 658–667, Jan. 1993.

[34] K. Takakura, H. Ohyama, A. Ueda, M. Nakabayashi, K. Hayama, K. Kobayashi, E. Simoen, A. Mercha, and C. Claeys, "Recovery behaviour resulting from thermal annealing in n-MOSFETs irradiated by 20 MeV protons," *Semicond. Sci. Technol.*, vol. 18, pp. 506–511, Jun. 2003.

[35] D. L. Griscom, "Thermal bleaching of x-ray-induced defect centers in high purity fused silica by diffusion of radiolytic molecular hydrogen," *J. Non-Cryst. Solids*, vol. 68, pp. 301–325, Nov. 1984.

[36] H. Wurzer, R. Mahnkopf, and H. Klose, "Annealing of degraded npn-transistors-mechanisms and modeling," *IEEE Trans. Electron Devices*, vol. 41, pp. 533–538, Apr. 1994.

[37] P. B. Parchinskii, S. I. Vlasov, and A. A. Nasirov, "The effect of γ-ray radiation on the characteristics of the interface between silicon and lead-borosilicate glass," *Semicond.s*, vol. 38, pp. 1304–1307, Nov. 2004.

[38] M. J. Aziz, "Stress effects on defects and dopant diffusion in Si," *Mater. Sci. Semicond. Process.*, vol. 4, pp. 397–403, Oct. 2001.

[39] E. Fretwurst, H. Herdan, G. Lindstrom, U. Pein, M. Rollwagen, H. Schatz, P. Thomsen, and R. Wunstorf, "Silicon detector developments for calorimetry: Technology and radiation damage," *Nucl. Instrum. Methods Phys. Res A*, vol. A288, pp. 1–12, Mar. 1990.

[40] E. Fretwurst, R. Grube, G. Lindstrom, and J. Nagel, "Development of large area silicon detectors: Special properties and radiation stability," *Nucl. Instrum. Methods Phys. Res A*, vol. A253, pp. 467–477, Jan. 1987.

[41] G. Lutz, *Semiconductor Radiation Detectors: Device Physics*. Berlin, Germany: Springer, 2007.

[42] M. Moll aus Ratzeburg, "Radiation Damage in Silicon Particle Detector-Microscopic Defects or Macroscopic Properties," Ph.D. dissertation, Dept. Elect. Eng., Harvard Univ., Cambridge, MA, 1999.

[43] K. K. Ng, *Complete Guide to Semiconductor Devices*. New York: McGraw-Hill, 1995.